Wang et al., http://www.jcb.org/cgi/content/full/jcb.201308146/DC1

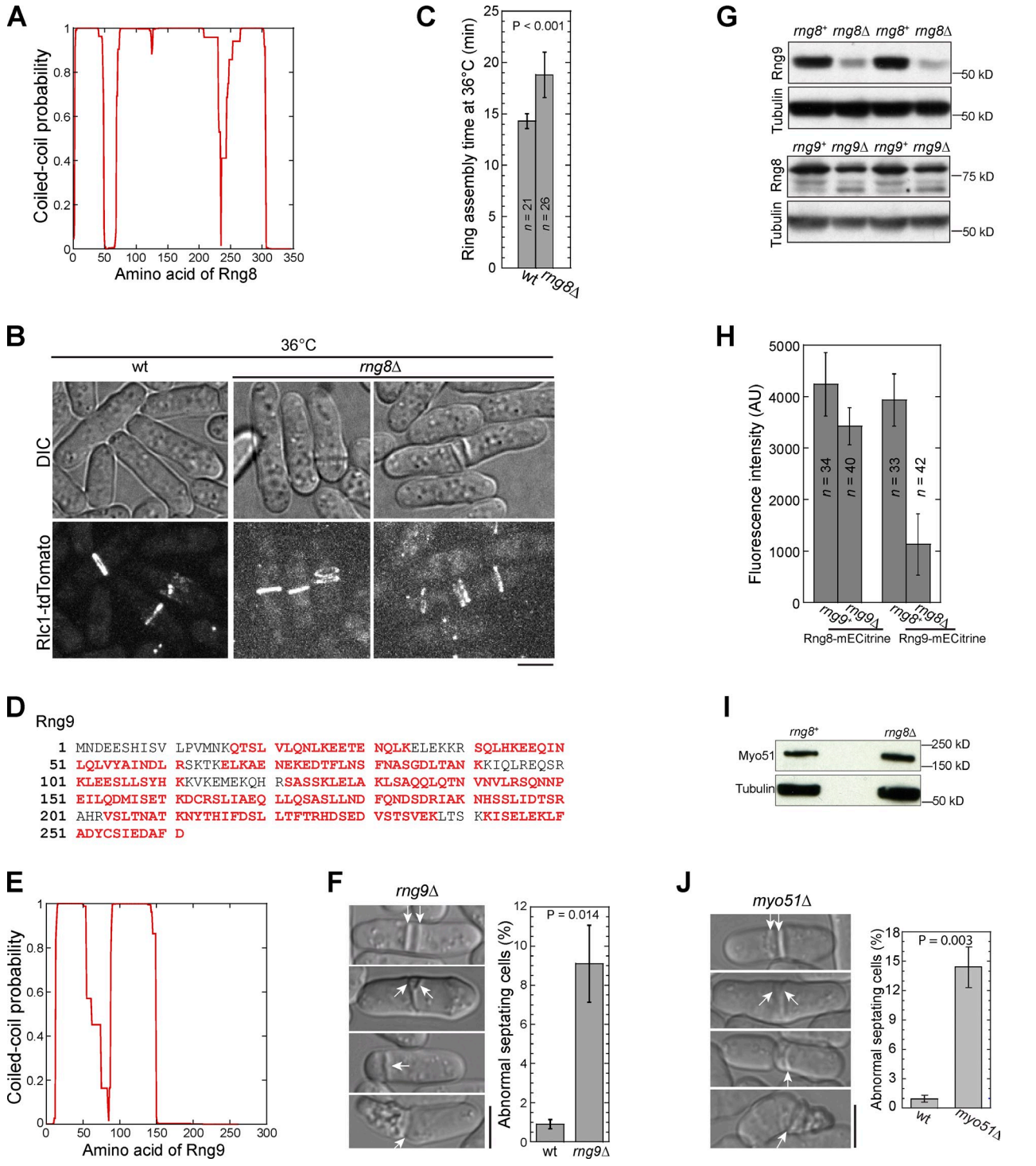

Figure S1. **The propensity for CC formation by Rng8 and Rng9, and cytokinesis defects in *rng8Δ*, *rng9Δ*, *and myo51Δ*.** (A) Probability of CC formation for Rng8 calculated using the program of Lupas et al. (1991) with a window size of 28. (B) Some *rng8Δ* cells form double contractile rings at the division site, which leads to aberrant septum formation at 36°C (Video 2). Note that images were selected from the time-lapse series similar to Video 2, and the fluorescence intensity is not comparable. (C) Time of contractile ring assembly in wt and *rng8Δ* cells at 36°C. (D) Sequence coverage (in red) for Rng9 in mass spectrometry of Rng8-S-tag affinity purification. (E) Probability of CC formation for Rng9 calculated using the program of Lupas et al. (1991) with a window size of 28. (F) DIC images and quantification of abnormal septating cells in *rng9Δ* cells at 36°C. $n > 300$ cells for each of three independent experiments. (G and H) Protein level of Rng8 and Rng9 revealed by Western blotting (G) or fluorescence microscopy (H). (G) Tubulin was used as the loading control and the samples were duplicated. (I) Myo51-3YFP protein level is normal in *rng8Δ* cells. Tubulin was used as the loading control. (J) DIC images and quantification of abnormal septating cells in *myo51Δ* cells at 36°C. $n > 300$ cells for each of three independent experiments. The arrows in F and J indicate aberrant septa. Error bars indicate 1 SD. Bars, 5 µm.

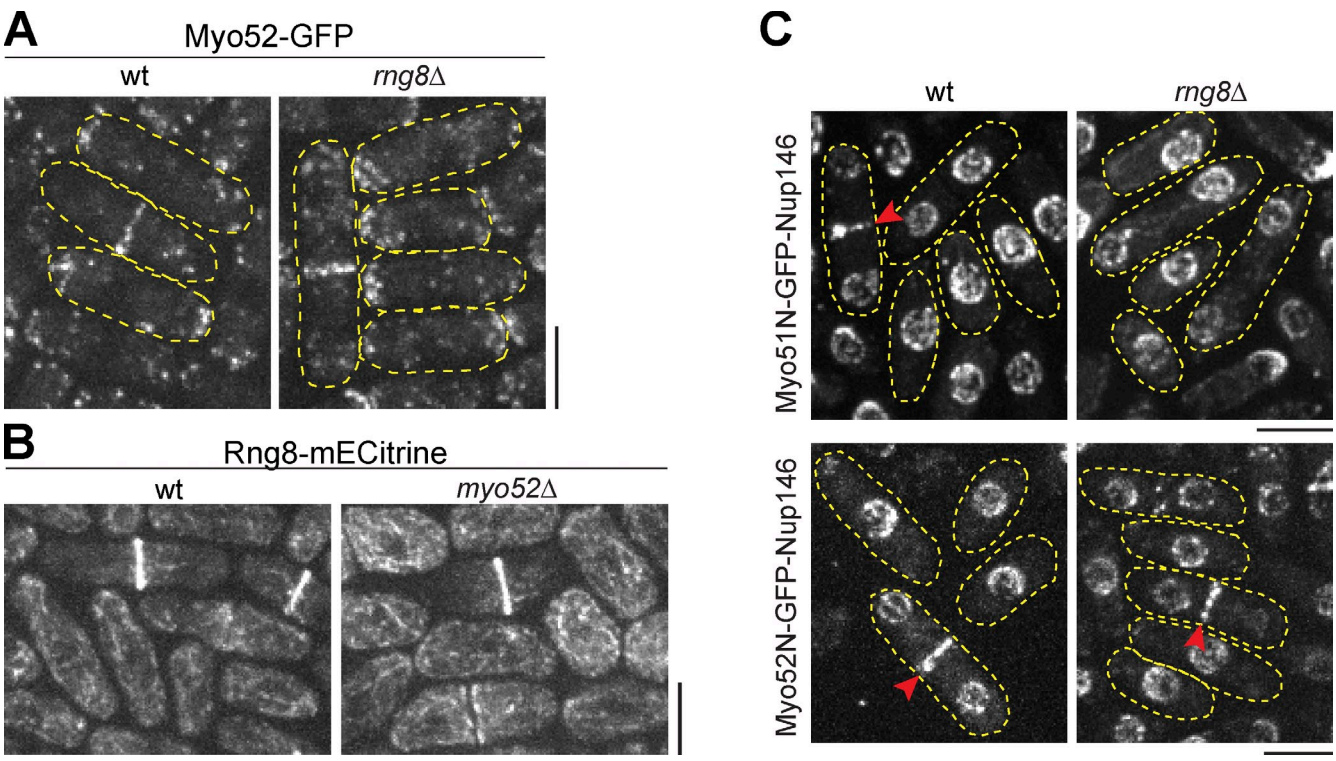

Figure S2. **Localizations of Myo52 and Rng8 are independent.** (A) Myo52 localization in wt and *rng8Δ* cells. (B) Rng8 localization in wt and *myo52Δ* cells. (C) *rng8Δ* disrupts the division site localization (arrowheads) of Myo51N-GFP-Nup146 but not Myo52N-GFP-Nup146. Cell boundaries are indicated by broken lines. Bars, 5 μm.

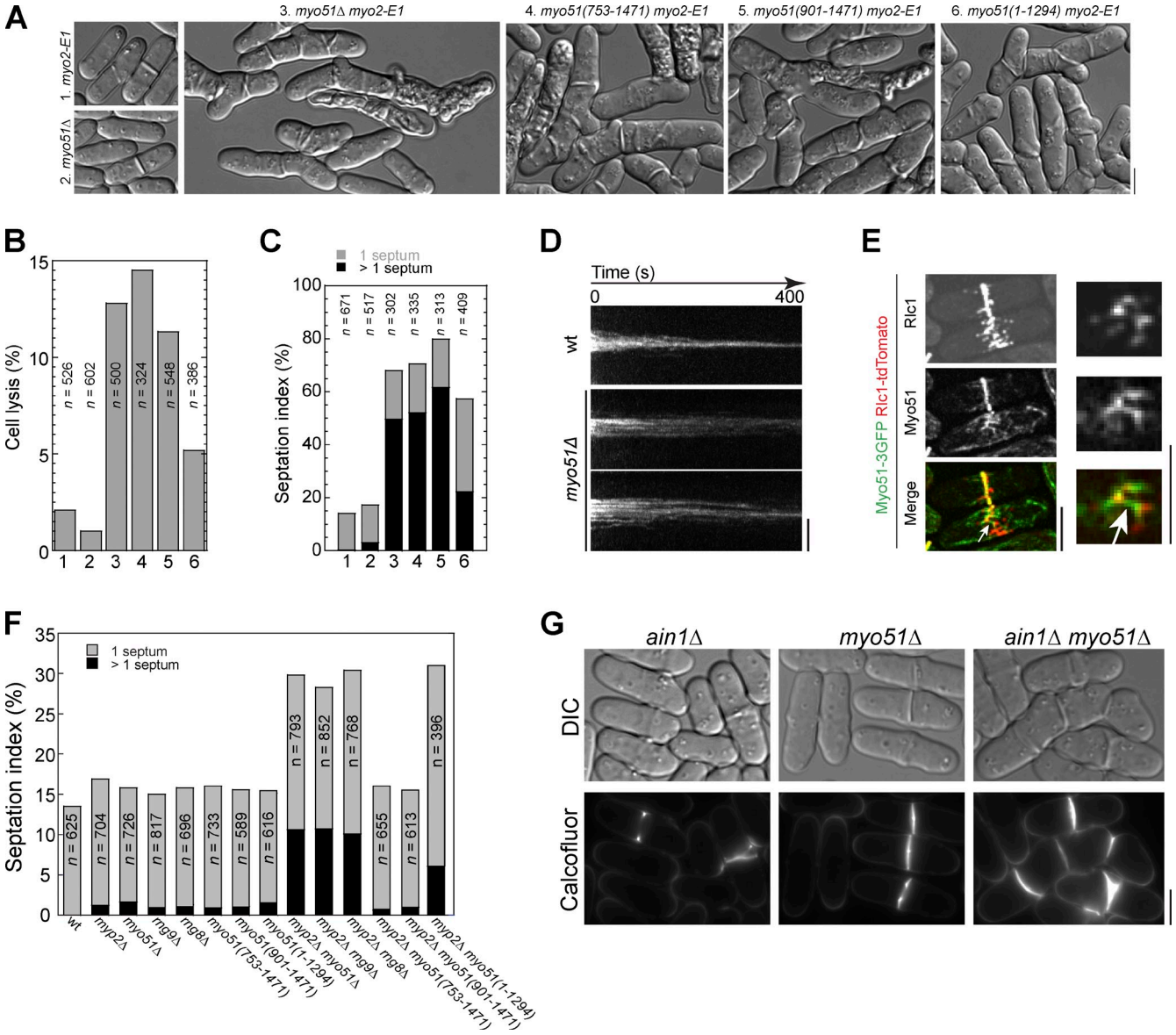

Figure S3. **Functions of Myo51 in cytokinesis and genetic interactions of *myo51* mutations with cytokinetic mutations.** (A–C) DIC images (A) and quantification (B and C) of synthetic genetic interactions between *myo2-E1* and *myo51* mutations mutants at 25°C. Quantification of cell lysis (B; lysed cell versus total cells) and the septation index (C) for mutants numbered as in A. (D) Kymographs showing node condensation over 400 s along the long axis of the cell (vertical) for *myo51*$^{+}$ or *myo51Δ* cells expressing Rlc1-tdTomato as the node marker at 23°C. Images were collected with 2-s intervals. (E) Localization of Myo51 meshwork (green) and Rlc1 nodes (red) in the same cell shown in maximum projection (left) or single focal plane (right, magnified region of the bottom cell). Arrows, two Rlc1 nodes connected by a short Myo51 cable. (F) Quantifications of the synthetic interactions between *rng8Δ*, *rng9Δ*, or *myo51* mutations and *myp2Δ*. Cells were grown at 36°C for 8 h before imaging. (G) Images of DIC and Calcofluor staining showing the synthetic interaction between *ain1Δ* and *myo51Δ*. Bars, 5 µm.

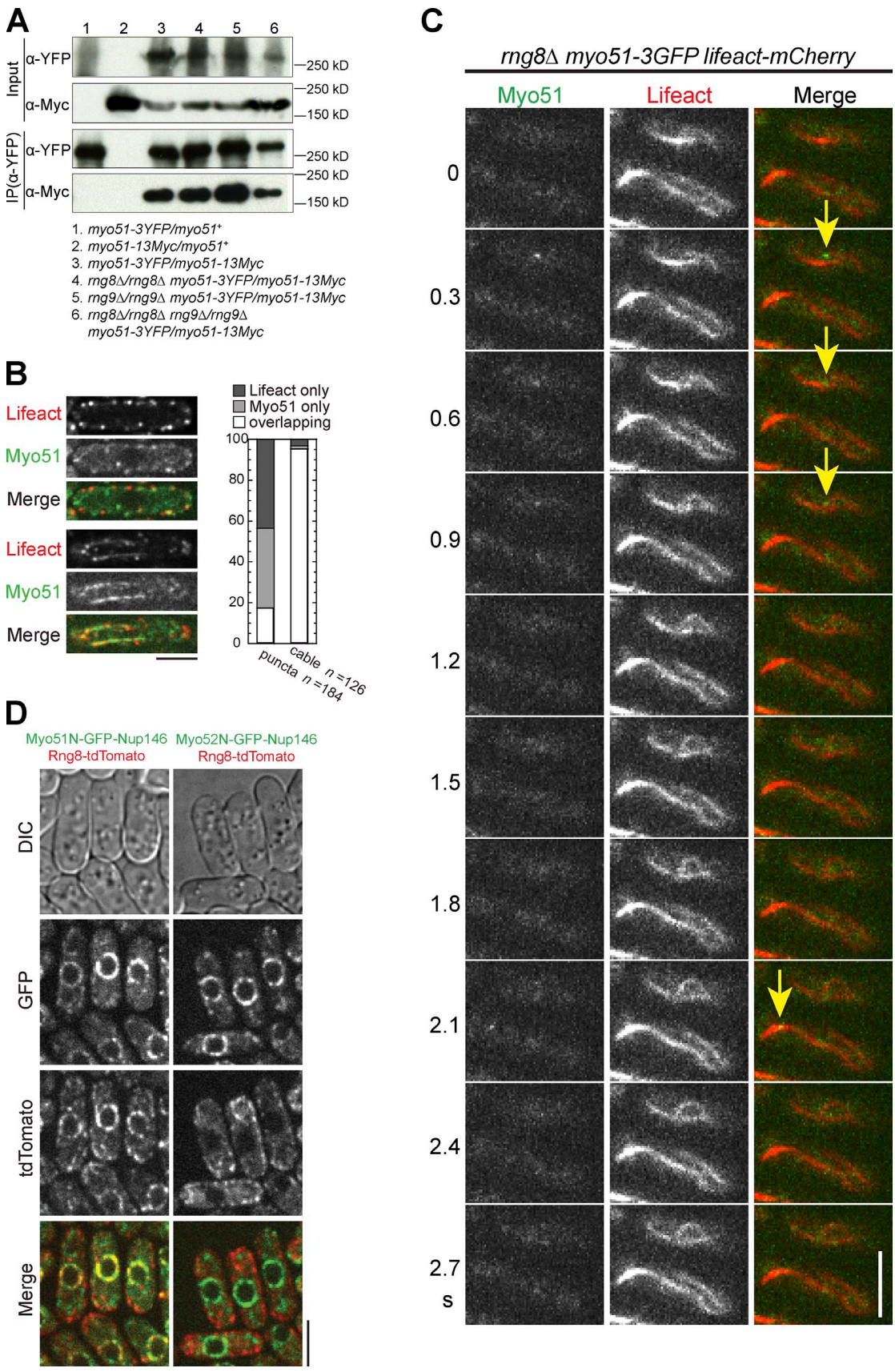

Figure S4. **Localization of Myo51 and movement of Myo51 speckles.** (A) FL Myo51 self-interaction does not depend on Rng8 or Rng9 in coIP assays of cell extracts from diploid cells. (B) Myo51 puncta mostly do not colocalize with actin patches. Micrographs of single focal plane (left) and quantification (right) of the colocalization of Myo51 puncta/cables with actin patches/cables, respectively. (C) Time course (in seconds) showing that two Myo51 speckles (yellow arrows) are unable to walk on actin cables in *rng8Δ* cells. Cells were treated with CK666 to reduce the interference of actin patches. Images were collected with 0.1-s intervals. (D) Rng8 colocalizes with Myo51N-GFP-Nup146 but not Myo52N-GFP-Nup146 to the nuclear envelope. The best focal planes are shown. Bars, 5 µm.

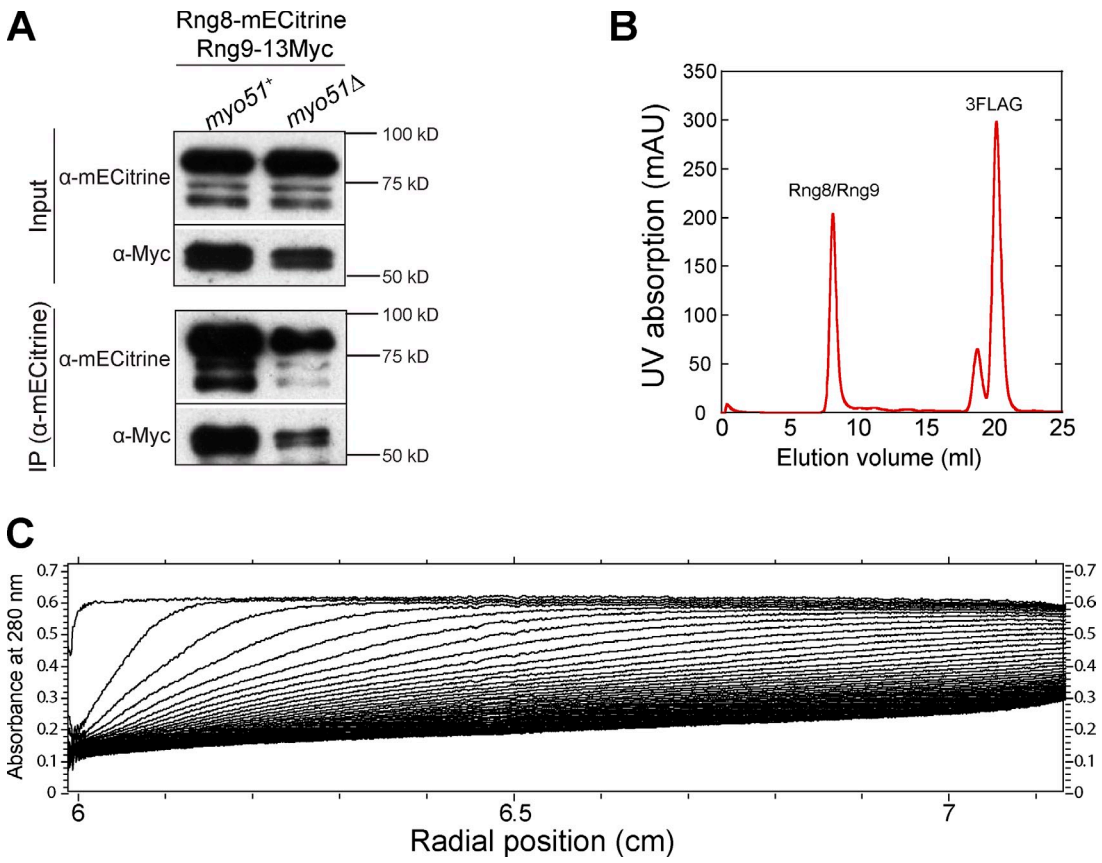

Figure S5. **Rng8 and Rng9 interact to form a big protein complex.** (A) Rng8-mECitrine still interacts with Rng9-13Myc without Myo51 in a coIP assay. (B) Elution of the purified Rng8–Rng9 complex without mixing with standard proteins from a calibrated gel filtration column. Note that the nonspecific small peak before the 3FLAG peak is <17 kD and contains no Rng8 or Rng9 by Western blotting. (C) Absorbance profile of the 21-μM Rng8–Rng9 protein sample for the analytical ultracentrifugation shown in Fig. 9 D.

Table S1. ***S. pombe* strains used in this study**

Strain name	Genotype	Figure/video/table/reference
JW3952	*h⁻ rng8-mECitrine-kanMX6 ade6-M210 leu1-32 ura4-D18*	Figs. 1 A, 2 (A, B, D, and E), 3 (C and F), S1 (G and H), and S2 B
JW3980	*rng8-mECitrine-kanMX6 sad1-mCFP-kanMX6 ade6-M210 leu1-32 ura4-D18*	Fig. 1 B
JW3981	*rng8-mEGFP-kanMX6 sad1-mCherry-natMX6 ade6-M210 leu1-32 ura4-D18*	Fig. 1 (C and D) and Video 1
JW81	*h⁻ ade6-210 ura4-D18 leu1-32*	Figs. 1 (E and F), 5 G, 7 A[a], S1 (F and J), S3 F, and S4 A[a]; Table S2; Wu et al., 2003
JW3772	*h⁻ rng8Δ::kanMX6 ade6-M210 leu1-32 ura4-D18*	Figs. 1 (E, F, I, and J), 5 G, and S3 F; and Table 1
JW1341	*h⁻ rlc1-tdTomato-natMX6 ade6-M210 leu1-32 ura4-D18*	Figs. 1 (G and H), 5 (A–F), S1 (B and C), and S3 D; and Videos 2 and 3; Vavylonis et al., 2008
JW3804	*rng8Δ::kanMX6 rlc1-tdTomato-natMX6 ade6-M210 ura4-D18 leu1-32*	Figs. 1 (G and H) and S1 (B and C); and Video 2
YDM74	*h⁻ myo2-E1 ade6-M216 his3-D1 leu1-32 ura4-D18*	Figs. 1 (I and J) and S3 (A–C); and Table 1; Balasubramanian et al., 1998
JW3925	*rng8Δ::kanMX6 myo2-E1 ade6 leu1-32 ura4-D18*	Fig. 1, I and J
JW4945	*h⁻ rng9-13Myc-natMX6 ade6-M210 leu1-32 ura4-D18*	Figs. 2 A and 3 D
JW4034	*h⁻ rng8-13Myc-hphMX6 ade6-M210 leu1-32 ura4-D18*	Figs. 2 A and 3 D
JW5019	*rng9-mECitrine-kanMX6 ade6-M210 leu1-32 ura4-D18*	Figs. 2 (A, B, D, and E), 3 C, and S1 (G and H)
JW5040	*rng8-mECitrine-kanMX6 rng9-13Myc-natMX6 ade6-M210 leu1-32 ura4-D18*	Figs. 2 A and S5 A
JW5046	*rng9-mECitrine-kanMX6 rng8-13Myc-hphMX6 ade6-M210 leu1-32 ura4-D18*	Fig. 2 A
JW5023	*h⁻ rng8Δ::kanMX6 rng9-mECitrine-kanMX6 ade6-M210 leu1-32 ura4-D18*	Figs. 2 B and S1 (G and H)
JW5082	*rng9Δ::natMX6 rng8-mECitrine-kanMX6 ade6-M210 leu1-32 ura4-D18*	Figs. 2 B and S1 (G and H)
JW3951	*h⁻ rng8-mEGFP-kanMX6 ade6-M210 leu1-32 ura4-D18*	Fig. 2 C
JW4948	*h⁻ rng9-mEGFP-hphMX6 ade6-M210 leu1-32 ura4-D18*	Fig. 2 C
JW1790	*h⁻ mid1-mECitrine-kanMX6 ade6-M210 leu1-32 ura4-D18*	Fig. 2 D; Laporte et al., 2011
JW4475	*rng8-tdTomato-kanMX6 myo51-3GFP-kanMX6 ade6 leu1-32 ura4-D18*	Fig. 3 A
MLY677	*h⁻ myo51-3YFP-kanMX6 ade6-M216 his3-D1 leu1-32 ura4-D18*	Figs. 3 (B and D), 4 B, 7 (B and C), 8 (E, G, and H), S1 I, and S4 A[a]; and Video 7; provided by M. Lord (University of Vermont, Burlington, VT)
JW4251	*rng8Δ::kanMX6 myo51-3YFP-kanMX6 ade6-M210 leu1-32 ura4-D18*	Figs. 3 B, 7 (B and C), and S1 I
JW5067	*rng9Δ::natMX6 myo51-3YFP-kanMX6 ade6-M216 leu1-32 ura4-D18*	Figs. 3 B and S4 A[a]
JW4343	*myo51Δ::ura4⁺ rng8-mECitrine-kanMX6 ade6-M210 leu1-32 ura4-D18*	Fig. 3 C
JW5018	*myo51Δ::ura4⁺ rng9-mECitrine-kanMX6 ade6-M210 leu1-32 ura4-D18*	Fig. 3 C
JW4422	*h⁻ myo51-3YFP-kanMX6 rng8-13Myc-hphMX6 ade6 leu1-32 ura4-D18*	Fig. 3 D
JW5084	*myo51-3YFP-kanMX6 rng9-13Myc-natMX6 ade6 leu1-32 ura4-D18*	Figs. 3 D and 4 E
MLY973	*h⁻ myo51-3GFP-kanMX6 ade6-M216 his3-D1 leu1-32 ura4-D18*	Fig. 3 E; provided by M. Lord
JW4406	*h⁻ myo51-mECitrine-kanMX6 ade6-M210 leu1-32 ura4-D18*	Fig. 3 F
JW4549	*h⁻ myo51(1–1,294)-3YFP-hphMX6 ade6-M210 leu1-32 ura4-D18*	Figs. 4 B, 5 G, 7 A[a], and S3 F; and Table 1
JW4550	*h⁻ myo51(1–900)-3YFP-hphMX6 ade6-M210 leu1-32 ura4-D18*	Fig. 4 B
JW4551	*h⁻ myo51(1–752)-3YFP-hphMX6 ade6-M210 leu1-32 ura4-D18*	Fig. 4 B
JW4810	*h⁻ kanMX6-Pmyo51-mECitrine-myo51 ade6-M210 leu1-32 ura4-D18*	Figs. 4 B and 7 D
JW4811	*h⁻ kanMX6-Pmyo51-mECitrine-myo51(753-1471) ade6-M210 leu1-32 ura4-D18*	Figs. 4 B and S3 F; and Table 1
JW4812	*h⁻ kanMX6-Pmyo51-mECitrine-myo51(901–1,471) ade6-M210 leu1-32 ura4-D18*	Figs. 4 B, 5 G, and S3 F; and Table 1
JW4813	*h⁻ kanMX6-Pmyo51-mECitrine-myo51(1,296–1,471) ade6-M210 leu1-32 ura4-D18*	Fig. 4 B
JW5576	*rng8Δ::hphMX6 kanMX6-Pmyo51-mECitrine-myo51 ade6-M210 leu1-32 ura4-D18*	Figs. 4, (C and D) and 7 D
JW5577	*rng8Δ::hphMX6 kanMX6-Pmyo51-mECitrine-myo51(753–1,471) ade6-M210 leu1-32 ura4-D18*	Fig. 4, C and D
JW5179	*myo51(1–1,294)-3YFP-hphMX6 rng9-13Myc-natMX6 ade6-M210 leu1-32 ura4-D18*	Fig. 4 E
JW5180	*myo51(1–900)-3YFP-hphMX6 rng9-13Myc-natMX6 ade6-M210 leu1-32 ura4-D18*	Fig. 4 E
JW5181	*myo51(1–752)-3YFP-hphMX6 rng9-13Myc-natMX6 ade6-M210 leu1-32 ura4-D18*	Fig. 4 E
JW5182	*kanMX6-Pmyo51-mECitrine-myo51 rng9-13Myc-natMX6 ade6-M210 leu1-32 ura4-D18*	Fig. 4 E
JW5183	*kanMX6-Pmyo51-mECitrine-myo51(753–1,471) rng9-13Myc-natMX6 ade6-M210 leu1-32 ura4-D18*	Fig. 4 E
JW5184	*kanMX6-Pmyo51-mECitrine-myo51(901–1,471) rng9-13Myc-natMX6 ade6-M210 leu1-32 ura4-D18*	Fig. 4 E
JW5185	*kanMX6-Pmyo51-mECitrine-myo51(1,296–1,471) rng9-13Myc-natMX6 ade6-M210 leu1-32 ura4-D18*	Fig. 4 E
JW5621	*h⁻ myo51Δ::natMX6 ade6-M210 leu1-32 ura4-D18* + pSM1255 [pREP41-Myo51-GFP]	Fig. 4 F
JW5622	*h⁻ myo51Δ::natMX6 ade6-M210 leu1-32 ura4-D18* + pSM1256 [pREP41-Myo52-GFP]	Fig. 4 F
JW5623	*h⁻ myo51Δ::natMX6 ade6-M210 leu1-32 ura4-D18* + pSM1247 [pREP41-M2IQ2-CC1-GTD2-GFP]	Figs. 4 F and 7 E
JW5626	*h⁻ ade6-M210 leu1-32 ura4-D18* + pSM1247 [pREP41-M2IQ2-CC1-GTD2-GFP]	Fig. 4 F
JW4419	*myo51Δ::ura4⁺ rlc1-tdTomato-natMX6 ade6-M210 leu1-32 ura4-D18*	Figs. 5 (A–F), S3 (D and G); and Videos 2 and 3
JW5548	*kanMX6-Pmyo51-mECitrine-myo51(901–1,471) rlc1-tdTomato-natMX6 ade6-M210 leu1-32 ura4-D18*	Fig. 5, A and B
JW5549	*kanMX6-Pmyo51-mECitrine-myo51(753–1,471) rlc1-tdTomato-natMX6 ade6-M210 leu1-32 ura4-D18*	Fig. 5, A and B
JW713	*h⁺ myp2-Δ2::kanMX6 ade6-M210 leu1-32 ura4-D18*	Figs. 5 G and S3 F; and Table 1
JW5017	*h⁻ rng9Δ::natMX6 ade6-M210 leu1-32 ura4-D18*	Figs. 5 G, S1 F, and S3 F; and Table 1
JW1273	*h⁺ myo51Δ::ura4⁺ade6-M210 leu1-32 ura4-D18*	Figs. 5 G, S1 J, and S3 F; Win et al., 2001
JW3836	*h⁻ rng8Δ::kanMX6 myp2-Δ2::kanMX6 ade6-M210 leu1-32 ura4-D18*	Figs. 5 G and S3 F
JW5121	*rng9Δ::natMX6 myp2-Δ2::kanMX6 ade6-M210 leu1-32 ura4-D18*	Figs. 5 G and S3 F

Table S1. ***S. pombe* strains used in this study** *(Continued)*

Strain name	Genotype	Figure/video/table/reference
JW4420	*myo51Δ::ura4⁺ myp2-Δ2::kanMX6 ade6-M210 leu1-32 ura4-D18*	Figs. 5 G and S3 F
JW5551	*kanMX6-Pmyo51-mECitrine-myo51(901–1,471) myp2-Δ2::kanMX6 ade6-M210 leu1-32 ura4-D18*	Figs. 5 G and S3 F
JW5642	*myo51(1–1,294)-3YFP-hphMX6 myp2-Δ2::kanMX6 ade6-M210 leu1-32 ura4-D18*	Figs. 5 G and S3 F
JW3573	*rlc1-tdTomato-natMX6 leu1⁺::GFP-psy1 ade6 ura4*	Fig. 5 H and Video 4; Ye et al., 2012
JW5143	*myo51Δ::ura4⁺ myp2-Δ2::kanMX6 rlc1-tdTomato-natMX6 leu1⁺::GFP-psy1 ade6-M21X ura4*	Fig. 5 H and Video 4
MBY7519	*h⁺ Pact1-lifeact-mGFP::leu1⁺ ade6-M210 leu1-32 ura4-D18*	Fig. 6 (A–E) and Video 5; Huang et al., 2012
JW5457	*myo51Δ::ura4⁺ Pact1-lifeact-mGFP::leu1⁺ ade6-M210 leu1-32 ura4-D18*	Fig. 6 (A–E) and Video 5
JW5769	*h⁺ myo51(1–1,294)-13Myc-natMX6 ade6-M216 leu1-32 ura4-D18*	Fig. 7 A[a]
JW5803	*h⁺ rng8Δ::kanMX6 myo51(1–1,294)-13Myc-natMX6 ade6-M216 leu1-32 ura4-D18*	Fig. 7 A[a]
JW5804	*h⁻ rng8Δ::kanMX6 myo51(1–1,294)-3YFP-hphMX6 ade6-M210 leu1-32 ura4-D18*	Fig. 7 A[a]
KV346	*h⁻ cdc12-3YFP-kanMX6 ade6-M216 leu1-32 ura4-D18 his3-D1*	Fig. 7, B and C; Wu and Pollard, 2005
JW5545	*h⁻ rng9-3YFP-kanMX6 ade6-M210 leu1-32 ura4-D18*	Fig. 7 C
JW5546	*h⁻ rng8-3YFP-kanMX6 ade6-M210 leu1-32 ura4-D18*	Fig. 7 C
JW4681	*h⁻ kanMX6-81nmt1-mECitrine-myo51 ade6-M210 leu1-32 ura4-D18*	Fig. 7 D
JW4757	*rng8Δ::kanMX6 kanMX6-81nmt1-mECitrine-myo51 ade6-M210 leu1-32 ura4-D18*	Fig. 7 D
JW5742	*rng8Δ::kanMX6 myo51Δ::ura4⁺ade6-M210 leu1-32 ura4-D18+* pSM1247 [pREP41-M2IQ2-CC1-GTD2-GFP]	Fig. 7 E
JW5242	*h⁺ myo51-3GFP-kanMX6 Pact1-lifeact-mCherry::leu1⁺ ade6-M216 leu1-32 ura4-D18*	Figs. 8 (A–D) and S4 B; and Video 6
JW4874	*for3Δ::kanMX6 myo51-3YFP-kanMX6 ade6 leu1-32 ura4-D18*	Fig. 8 E
JW5399	*rng8Δ::kanMX6 myo51-3GFP-kanMX6 Pact1-lifeact-mCherry::leu1⁺ ade6-M21X leu1-32 ura4-D18*	Figs. 8 F and S4 C
JW4652	*h⁻ rng8Δ::kanMX6 myo51-3YFP-kanMX6 ade6-M216 leu1-32 ura4-D18*	Figs. 8 (G and H) and S4 A[a]; and Video 7
YSM2297	*h⁻ ura4-294::nmt82-myo51N-GFP-nup146-ura4⁺*	Figs. 8 (I–K) and S2 C; and Video 8
JW5398	*rng8Δ::kanMX6 ura4-294::nmt82-myo51N-GFP-nup146-ura4⁺ ade6-M210 leu1-32*	Figs. 8 (J and K) and S2 C
JW5401	*rng8Δ::hphMX6 ura4-294::nmt82-myo51N-GFP-nup146-ura4⁺ ade6-M210 leu1-32*	Fig. 8 K
JW5441	*rng8Δ::kanMX6 ura4-294::nmt82-myo52N-GFP-nup146-ura4⁺ ade6-M210 leu1*	Figs. 8 K and S2 C
JW5448	*rng8-tdTomato-kanMX6 ura4-294::nmt82-myo52N-GFP-nup146-ura4⁺ ade6-M210 leu1*	Figs. 8 K, S2 C, and S4 D
JW5385	*myo51Δ::ura4⁺ kanMX6-3nmt1-3FLAG-rng8 kanMX6-3nmt1-rng9-13Myc-natMX6 ade6-M210 leu1-32 ura4-D18*	Figs. 9 (A–D) and S5 C
JW2923	*myp2-Δ2::kanMX6 rlc1-tdTomato-natMX6 leu1⁺::GFP-psy1 ade6 ura4*	Video 4; Ye et al., 2012
JW5637	*myo51Δ::ura4⁺ rlc1-tdTomato-natMX6 leu1⁺::GFP-psy1 ade6-M210 leu1-32 ura4*	Video 4
JW4619	*h⁻ rng8-S-tag-kanMX6 ade6-M210 leu1-32 ura4-D18*	Fig. S1 D and Table S2
FC857	*h⁻ myo52-GFP-kanMX6 ade6-M210 leu1-32 ura4-D18*	Fig. S2 A; Feierbach and Chang, 2001
JW4249	*rng8Δ::kanMX6 myo52-GFP-kanMX6 ade6-M210 leu1-32 ura4-D18*	Fig. S2 A
JW4344	*myo52Δ::ura4⁺ rng8-mECitrine-kanMX6 ade6-M210 leu1-32 ura4-D18*	Fig. S2 B
JW5499	*h⁻ myo51Δ::natMX6 ade6-M210 leu1-32 ura4-D18*	Fig. S3, A–C; and Table 1
JW5635	*myo51Δ::natMX6 myo2-E1 ade6-M210 leu1-32 ura4-D18*	Fig. S3, A–C
JW5599	*myo2-E1 kanMX6-Pmyo51-mECitrine-myo51(753–1,471) ade6 leu1-32 ura4-D18*	Fig. S3, A–C
JW5600	*myo2-E1 kanMX6-Pmyo51-mECitrine-myo51(901–1,471) ade6 leu1-32 ura4-D18*	Fig. S3, A–C
JW5601	*myo2-E1 myo51(1–1,294)-3YFP-hphMX6 ade6 leu1-32 ura4-D18*	Fig. S3, A–C
JW5571	*rlc1-tdTomato-natMX6 myo51-3GFP-kanMX6 ade6-M216 leu1-32 ura4-D18*	Fig. S3 E
JW5550	*kanMX6-Pmyo51-mECitrine-myo51(753–1,471) myp2-Δ2::kanMX6 ade6-M210 leu1-32 ura4-D18*	Fig. S3 F
JW1861	*ain1Δ::ura4⁺ rlc1-tdTomato-natMX6 ade6-M210 ura4-D18 leu1-32*	Fig. S3 G and Table 1
JW5086	*ain1Δ::ura4⁺ myo51Δ::kanMX4 rlc1-tdTomato-natMX6 ade6 leu1-32 ura4-D18*	Fig. S3 G
JW4503	*h⁺ myo51-13Myc-natMX6 ade6-210 leu1-32 ura4-D18*	Fig. S4 A[a]
JW4653	*h⁺ rng8Δ::kanMX6 myo51-13Myc-natMX6 ade6-210 leu1-32 ura4-D18*	Fig. S4 A[a]
JW5238	*h⁺ rng8Δ::kanMX6 rng9Δ::natMX6 myo51-13Myc-natMX6 ade6-210 leu1-32 ura4-D18*	Fig. S4 A[a]
JW5239	*h⁺ rng9Δ::natMX6 myo51-13Myc-natMX6 ade6-210 leu1-32 ura4-D18*	Fig. S4 A[a]
JW5237	*h⁻ rng8Δ::kanMX6 rng9Δ::natMX6 myo51-3YFP-kanMX6 ade6-M216 leu1-32 ura4-D18*	Fig. S4 A[a]
JW729	*h⁺ ade6-M210 leu1-32 ura4-D18*	Fig. S4 A[a]; Wu et al., 2003
JW5418	*rng8-tdTomato-kanMX6 ura4-294::nmt82-myo51N-GFP-nup146-ura4⁺ ade6-M210 leu1-32*	Fig. S4 D
JW5234	*myo51Δ::ura4⁺ rng8-mECitrine-kanMX6 rng9-13Myc-natMX6 ade6-M210 leu1-32 ura4-D18*	Fig. S5 A
JW2254	*h⁺ rlc1Δ::kanMX6 ade6-M210 leu1-32 ura4-D18*	Table 1
MBY925	*h⁻ myo2-ΔIQ1ΔIQ2::ura4⁺ leu1-32 ura4-D18*	Table 1; D'souza et al., 2001
JW1279	*h⁻ cdc3-124 his7-366 ade6-M210 leu1-32 ura4-D18*	Table 1
YDM136	*h⁻ cdc8-110 his3-D1 leu1-32 ura4-D18*	Table 1; Balasubramanian et al., 1992
YDM821	*h⁺ clp1::ura4⁺ ade6-M216 leu1-32 ura4-D18*	Table 1; Jin et al., 2007
JW1636	*h⁺ mid1-6 ade6-M210 leu1-32 ura4-D18*	Table 1
JW2255	*h⁺ mid1-366 ade6-M210 leu1-32 ura4-D18*	Table 1

[a]Because diploid cells are not stable for long-term storage and we only used freshly made diploid strains for the coIP assays in Fig. 7A and Fig. S4 A, only the parental strains are listed.

Table S2. **Proteins identified in mass spectrometry of affinity-purified Rng8-S-tag from *S. pombe*[a]**

Protein[b]	Number of significant matches	Number of significant sequences	Coverage	Protein description
			%	
Rng8	76	29	61	Uncharacterized protein SPAC4H3.14c
Rng9	41	18	80	Uncharacterized protein SPBP8B7.02
SPAC12G12.07c	1	1	<5	Uncharacterized protein
Mnn9	1	1	<5	Mannan polymerase complex subunit
Chs1	1	1	<5	Chitin synthase 1
SPCC550.11	2	2	<5	Probable importin
Arp2	1	1	<5	Actin-related protein 2
Pmm1	1	1	<5	Phosphomannomutase
Nrs1	1	1	<5	Probable asparagine-tRNA ligase
Gly1	1	1	<5	Probable low-specificity L-threonine aldolase

[a]Protein samples purified from wt (JW81) and *rng8-S-tag-kanMX6* (JW4619) were both analyzed by mass spectrometry. Identified proteins listed in this table are JW4619 specific.
[b]The database for this blast was SwissProt.

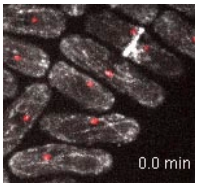

Video 1. **Rng8 localization during cytokinesis.** The SPB is marked with Sad1-mCherry. The interval is 1.5 min in time-lapse confocal microscopy (UltraVIEW ERS; PerkinElmer). The maximum intensity projections from 11 slices spaced at 0.4 µm at each time point are merged and shown. This video corresponds to Fig. 1 C. Display rate: 8 frames per second (fps).

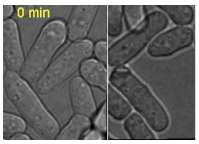

Video 2. **Contractile ring assembly, maturation, and constriction in wt (left), *rng8Δ* (middle), and *myo51Δ* (right) cells expressing Rlc1-tdTomato at 36°C.** The interval is 1 min in time-lapse confocal microscopy (UltraVIEW Vox CSUX1; PerkinElmer). Top, DIC. Bottom, Rlc1-tdTomato, with maximum intensity projections from 11 slices spaced at 0.5 µm at each time point. This video corresponds to Fig. S1 B. Display rate: 8 fps.

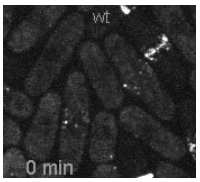

Video 3. **Node condensation in wt (left) and *myo51Δ* (right) cells expressing Rlc1-tdTomato at 23°C.** The interval is 1 min in time-lapse confocal microscopy (UltraVIEW ERS; PerkinElmer). The maximum intensity projections from 11 slices spaced at 0.4 µm at each time point are merged and shown. This video corresponds to Fig. 5 A. Display rate: 8 fps.

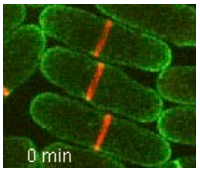

Video 4. **Contractile ring constriction and membrane invagination in wt (left), *myo51Δ* (left middle), *myp2Δ* (right middle), and *myo51Δ myp2Δ* mutant (right).** Rlc1-tdTomato is used as the ring marker, and GFP-Psy1 as the plasma membrane marker. The interval is 1 min in time-lapse confocal microscopy (UltraVIEW ERS; PerkinElmer). The maximum intensity projections from 11 slices spaced at 0.4 µm at each time point are merged and shown. This video corresponds to Fig. 5 H. Display rate: 8 fps.

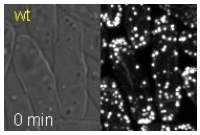

Video 5. **Contractile ring formation in wt (left two panels) or *myo51Δ* (right two panels) cells expressing Lifeact-mGFP.** The interval is 1 min in time-lapse confocal microscopy (UltraVIEW Vox CSUX1; PerkinElmer). For each strain, DIC is shown on the left. The maximum intensity projections of the fluorescence images from 13 slices spaced at 0.5 µm at each time point are merged and shown on the right. This video corresponds to Fig. 6 A. Display rate: 8 fps.

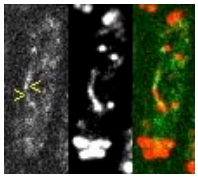

Video 6. **Myo51-3GFP puncta moving along actin filament labeled with Lifeact-mCherry.** Two cells (top and bottom) imaged at a single focal plane for GFP (left), mCherry (middle), and merged (right) channels are shown. The start and end of the puncta movement were marked with < and > in the GFP channel. The interval is 0.1 s in time-lapse confocal microscopy (UltraVIEW Vox CSUX1; PerkinElmer). The length of the movie is 2.4 s. This video corresponds to Fig. 8 A. Display rate: 6 fps.

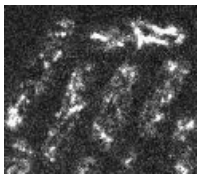

Video 7. **Myo51-3YFP speckles do not move continuously and directionally in *rng8Δ* cells.** *rng8*$^{+}$ (left) and *rng8Δ* cells (right) imaged at a single focal plane for YFP channel are shown. The interval is 0.1 s in time-lapse confocal microscopy (UltraVIEW Vox CSUX1; PerkinElmer). The brightness setting is higher for *rng8Δ* cells to visualize the Myo51 speckles clearly. The length of the movie is 8 s. This video corresponds to Fig. 8 G. Display rate: 6 fps.

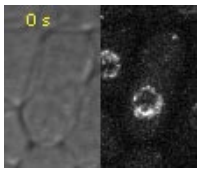

Video 8. **Nuclear movement in cells expressing Myo51N-GFP-Nup146 treated with MBC for 15 min.** The interval is 10 s in time-lapse confocal microscopy (UltraVIEW ERS; PerkinElmer). DIC is shown on the left. The maximum intensity projections from 13 slices spaced at 0.5 µm from the GFP channel at each time point are merged and shown on the right. This video corresponds to Fig. 8 I. Display rate: 8 fps.

References

Balasubramanian, M.K., D.M. Helfman, and S.M. Hemmingsen. 1992. A new tropomyosin essential for cytokinesis in the fission yeast *S. pombe*. *Nature*. 360:84–87. http://dx.doi.org/10.1038/360084a0

Balasubramanian, M.K., D. McCollum, L. Chang, K.C. Wong, N.I. Naqvi, X. He, S. Sazer, and K.L. Gould. 1998. Isolation and Characterization of New Fission Yeast Cytokinesis Mutants. *Genetics*. 149:1265–1275.

D'souza, V.M., N.I. Naqvi, H. Wang, and M.K. Balasubramanian. 2001. Interactions of Cdc4p, a myosin light chain, with IQ-domain containing proteins in *Schizosaccharomyces pombe*. *Cell Struct. Funct.* 26:555–565. http://dx.doi.org/10.1247/csf.26.555

Feierbach, B., and F. Chang. 2001. Roles of the fission yeast formin for3p in cell polarity, actin cable formation and symmetric cell division. *Curr. Biol.* 11:1656–1665. http://dx.doi.org/10.1016/S0960-9822(01)00525-5

Huang, J., Y. Huang, H. Yu, D. Subramanian, A. Padmanabhan, R. Thadani, Y. Tao, X. Tang, R. Wedlich-Soldner, and M.K. Balasubramanian. 2012. Nonmedially assembled F-actin cables incorporate into the actomyosin ring in fission yeast. *J. Cell Biol.* 199:831–847. http://dx.doi.org/10.1083/jcb.201209044

Jin, Q.-W., S. Ray, S.H. Choi, and D. McCollum. 2007. The nucleolar Net1/Cfi1-related protein Dnt1 antagonizes the septation initiation network in fission yeast. *Mol. Biol. Cell*. 18:2924–2934. http://dx.doi.org/10.1091/mbc.E06-09-0853

Laporte, D., V.C. Coffman, I.-J. Lee, and J.-Q. Wu. 2011. Assembly and architecture of precursor nodes during fission yeast cytokinesis. *J. Cell Biol.* 192:1005–1021. http://dx.doi.org/10.1083/jcb.201008171

Lupas, A., M. Van Dyke, and J. Stock. 1991. Predicting coiled coils from protein sequences. *Science*. 252:1162–1164. http://dx.doi.org/10.1126/science.252.5009.1162

Vavylonis, D., J.-Q. Wu, S. Hao, B. O'Shaughnessy, and T.D. Pollard. 2008. Assembly mechanism of the contractile ring for cytokinesis by fission yeast. *Science*. 319:97–100. http://dx.doi.org/10.1126/science.1151086

Win, T.Z., Y. Gachet, D.P. Mulvihill, K.M. May, and J.S. Hyams. 2001. Two type V myosins with non-overlapping functions in the fission yeast *Schizosaccharomyces pombe*: Myo52 is concerned with growth polarity and cytokinesis, Myo51 is a component of the cytokinetic actin ring. *J. Cell Sci.* 114:69–79.

Wu, J.-Q., and T.D. Pollard. 2005. Counting cytokinesis proteins globally and locally in fission yeast. *Science*. 310:310–314. http://dx.doi.org/10.1126/science.1113230

Wu, J.-Q., J.R. Kuhn, D.R. Kovar, and T.D. Pollard. 2003. Spatial and temporal pathway for assembly and constriction of the contractile ring in fission yeast cytokinesis. *Dev. Cell*. 5:723–734. http://dx.doi.org/10.1016/S1534-5807(03)00324-1

Ye, Y., I-J. Lee, K.W. Runge, and J.-Q. Wu. 2012. Roles of putative Rho-GEF Gef2 in division-site positioning and contractile-ring function in fission yeast cytokinesis. *Mol. Biol. Cell*. 23:1181–1195. http://dx.doi.org/10.1091/mbc.E11-09-0800